nature communications

Article

https://doi.org/10.1038/s41467-024-55650-8

Ocean's largest chlorophyll-rich tongue is extending westward (2002–2022)

Received: 2 April 2024

Accepted: 19 December 2024

Shuaixing Peng[1,2], Xiaolong Yu[1,2], Zhongping Lee[1], Hongyang Lin[1], Xin Liu[1], Minhan Dai[1] & Shaoling Shang[1]

Upwelling in the Equatorial Pacific nurtures an expansive, westward-stretching chlorophyll-rich tongue (CRT), supporting 18% of the annual global new production. Surrounding the CRT are the oligotrophic subtropical gyres to the north and south, which are suggested to be expanding under global warming. Yet, how this productive CRT has changed, expanding or contracting, remains unknown. By applying the empirical mode decomposition (EMD) method to 20-year monthly measurements of chlorophyll-a concentration from MODIS-Aqua satellite (2002-2022), we demonstrate that the CRT exhibited a significant westward extension, at an average expanding rate of 1.87 (± 0.82) × 10^5 km^2/yr. The westward extension of the CRT is attributed to strengthened equatorial upwelling and a strengthened South Equatorial Current from 2002 to 2022, driven by intensified easterly trade winds as the Pacific Decadal Oscillation predominantly remains in its negative phase during this period. Interestingly, EMD analysis on central locations of the Pacific gyres suggested simultaneous extension of the gyres and the CRT during 2002-2022, with the gyres extending poleward. Our findings imply a broader cover of productive water along the equator, while its impact on tropical climate, ecosystems, and carbon cycle deserves further investigation.

Owing to the upwelling of nutrient- and carbon dioxide (CO_2)-rich waters, the equatorial Pacific Ocean emerges as the largest oceanic source of atmospheric CO_2, as well as a highly productive area sustaining about 18% of the global oceanic new production[1–3]. The upwelling-supported phytoplankton enrichment forms a tongue of high chlorophyll concentration, spreading westward from the east Peruvian coast to beyond 180°W[4]. Specifically, the formation of this chlorophyll-rich tongue (CRT) is sustained by the local supply of nutrients facilitated by upwelling caused by the trade-wind-driven divergence of the Ekman flow at the equator[5,6], as well as the westward advection of nutrient-rich water via the South Equatorial Current (SEC) originating from coastal upwelling off Peru[7]. The extent and intensity of the CRT vary with seasons and years[2], with its interannual variability primarily influenced by El Niño-Southern Oscillation (ENSO)[8–12]. The long-term variation in the CRT remains unclear, despite notable changes in atmospheric circulation, ocean currents, and ecosystems observed in the equatorial Pacific[13–19]. For example, a pronounced strengthening in Pacific trade winds during 1992-2011 is observed, which is considered to be sufficient to account for the cooling of the tropical Pacific in that period[14]; the North Equatorial Current having intensified in the western Pacific Ocean during the period of the 1900s–2000s[17]. Potential changes in CRT are noteworthy, especially considering that the oligotrophic subtropical gyres in the global ocean were suggested to be expanding over the last two decades due to strengthened vertical stratification induced by global warming[20–23]. It thus prompts a crucial question: is the CRT in the equatorial Pacific, located right in-between the expanding North and South Pacific Subtropical Gyres, inevitably shrinking? The changes in CRT may have consequences for ecosystems[9], heat exchanges[24], and air-sea CO_2 fluxes[2], making it particularly important to understand CRT dynamics amidst ongoing global climate change.

In this study, we endeavored to address this question by applying the empirical mode decomposition (EMD) method to a 20-year

---

[1] State Key Laboratory of Marine Environmental Science, College of Ocean and Earth Sciences, Xiamen University, Xiamen, Fujian 361102, China. [2] These authors contributed equally: Shuaixing Peng, Xiaolong Yu. e-mail: slshang@xmu.edu.cn

(August 2002 - July 2022) monthly time series of surface chlorophyll-a concentration (Chl) derived from Moderate-resolution Imaging Spectroradiometer aboard the Aqua satellite (MODIS-Aqua). The potential forcings underlying CRT changes were discussed based on winds and ocean currents data of the same period.

Results

Westward extension of the chlorophyll-rich tongue in the equatorial Pacific

Here, we define the boundary of the CRT as the Chl isoline of 0.1 mg/m^3, with the climatology boundary delineated in Fig. 1a (see the black curve). Clearly, within the boundary of the CRT are the poleward equatorial surface water divergence and the westward SEC (Fig. 1b).

The monthly variations of the area of CRT from 2002 to 2022 were first obtained from Chl measurements by MODIS-Aqua (Fig. 2a). A linear trend fitting was first applied to this time series of CRT area, which suggests no statistically significant trend ($P = 0.58$, see the red line in Fig. 2a). The EMD, which is powerful in detecting trend[25], was then carried out to decompose the CRT area time series into seasonal and interannual components, as well as a residual trend component, as the focus of this analysis is on distinguishing between these variabilities and the residual trend (see “Methods” and Supplementary Fig. 1). Following the approach of Serio et al. [26], we obtained an estimate of the weight of the amplitude of the trend, which contributes 9% to the variability of the total signal, while the interannual and seasonal components explain 59% and 32%, respectively.

The seasonal variation of the CRT area highlights peaks of the CRT area in January and May-June and a minimum in October-November (see the insert figure in Fig. 2b). This pattern is in general in phase with the known seasonal cycle of the equatorial current system[27].

The interannual variability of the CRT area, the dominant component, is negatively correlated with the Multivariate ENSO Index (MEI) ($R = -0.65$, $P < 0.01$) (Fig. 2c), which is consistent with prior findings that the CRT’s interannual variability is primarily influenced by ENSO[8,9,12,28,29]. For example, the notable reduction in size of the CRT in 2016 coincided with an intense El Niño event characterized by a positive MEI (Fig. 2c). During strong El Niño events like 2016, anomalous westerly winds in the tropical western Pacific suppress the westward advection and lead to weakened equatorial upwelling[2,30–33], which hampers the extension of the CRT.

Interestingly, the residual component demonstrates a notable increasing trend of the CRT area from 2002 to 2022 (Fig. 2d). The rate of CRT expansion is 1.87 (±0.82) × 10^5 km^2/yr, equivalent to an increase of 0.8% per year. Notably, a similar increasing trend is also observed when applying the same EMD to a longer record of CRT area from 1997-2023, calculated from a merged Chl dataset derived from multiple ocean color missions (see Supplementary Fig. 2). Furthermore, the application of the ensemble empirical mode decomposition (EEMD) method[34] to the CRT area time series in 2002–2022 results in a similar expanding rate (1.31 (±2.46) × 10^5 km^2/yr) (see Supplementary Fig. 3). The confidence interval appears wide over most of the study period due to a higher standard deviation, which results from random white noise added in the EEMD analysis and is not material to the direction of the residual trend.

To determine the direction of the CRT extension, we applied EMD analysis to the time series of the CRT’s western, northern, and southern boundaries (see the definition of boundaries in “Methods”). The western boundary exhibits a significant westward movement trend from 2002 to 2022, with a rate of 0.43 (±0.23) °/yr (Fig. 3a). In contrast, both the northern and southern boundaries move northward slightly at almost the same rate, which is an order of magnitude lower than that of westward extending (Fig. 3b, c). Thus, their contributions to the expansion of CRT could be largely neglected. Therefore, the expansion of CRT is predominantly attributed to the westward extension. With

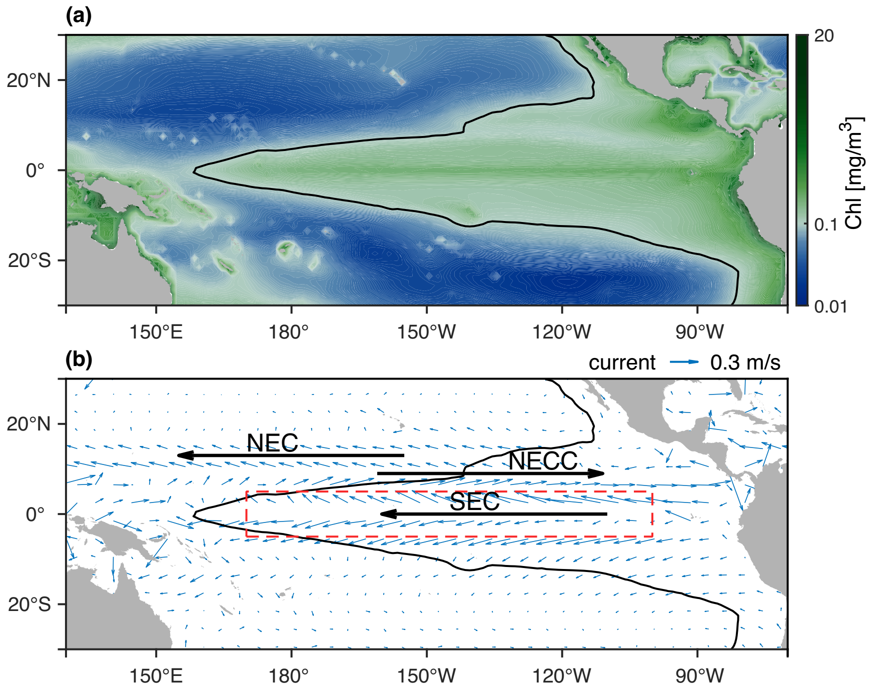

Fig. 1 | Illustration of the chlorophyll-rich tongue (CRT) and spatial distributions of ocean current fields in the equatorial Pacific. Climatological mean (**a**) surface chlorophyll concentration (Chl, mg/m^3) and (**b**) current fields (m/s) between August 2002 and July 2022. The CRT climatology boundary is delineated with the black curve, representing the Chl isoline of 0.1 mg/m^3. The major surface currents are shown in solid black arrows in (**b**), including North Equatorial Current (NEC), North Equatorial Counter-Current (NECC) and South Equatorial Current (SEC). The area enclosed by the red dashed lines in (**b**) denotes the central positions of SEC (5° S-5° N, 170° E-100° W).

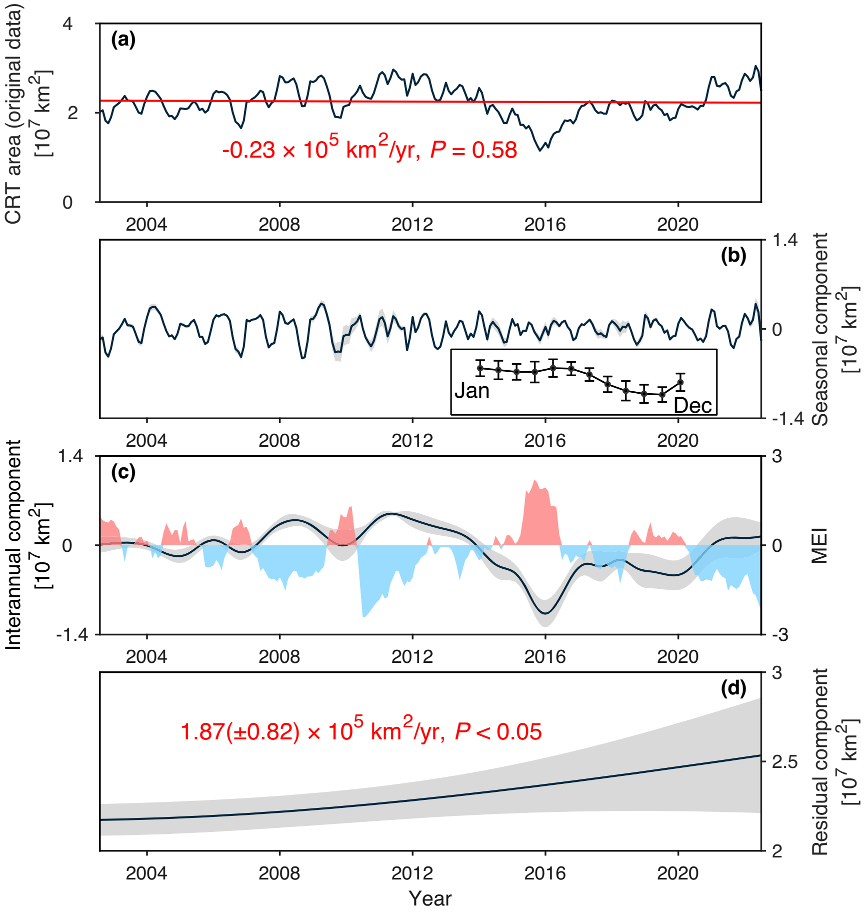

Fig. 2 | Decomposition of the monthly time series of the chlorophyll-rich tongue (CRT) area using empirical mode decomposition (EMD). a The original 20-year monthly time series of the CRT area (the solid black line), its linear fitting trend (solid red line), and its decomposition into (**b**) seasonal, (**c**) interannual, and (**d**) residual components. Variabilities of high-frequency (< 2 year) were combined as the seasonal component; the components of low-frequency (> 8 years) were combined into the interannual component, because the 20-year time span of the CRT area time series inhibits the decomposition of decadal variability with physical meaning. The seasonal pattern of the CRT area is inserted in (**b**), with the solid line and error bar representing the mean CRT area and the standard deviation of each month, respectively. The temporal variation of the Multivariate ENSO Index (MEI) is also included in (**c**), with the red and blue shadings indicating El Niño and La Niña, respectively. The gray shading represents a range of two standard deviations, equivalent to a 95% confidence limit (see "Methods").

the assumption that the average distance between the northern and southern boundaries is the average width of CRT, which is approximately 21.9°, the CRT expansion contributed by the westward extension would be roughly 1.08×10^5 km^2/yr. This estimated expanding rate is comparable to that obtained from the EMD analysis (i.e., 1.87×10^5 km^2/yr, Fig. 2d).

In addition, the evolution of the monthly mean CRT area from year to year confirms the expansion of CRT from 2002 to 2022 (see color curves in Fig. 4a). For a better and straightforward illustration, we show the comparison of the averaged CRT area in the last five years (2018–2022) (the magenta area in Fig. 4b) to that in the first five years (2003–2007) (the light blue area in Fig. 4b), which features a significant westward extension. Note that the CRT area illustrated in Fig. 4a has deducted the prominent interannual component to reinforce the long-term evolution. Based on Fig. 4b, a purely graphical estimation of the expanding rate of the CRT area, by counting the difference in magenta and light blue pixels, is obtained (1.07×10^5 km^2/yr). This estimate is overall consistent with that derived from the EMD analysis (1.87×10^5 km^2/yr), providing an independent confirmation of the estimated expanding rate by the EMD analysis. Taken together, there is a high degree of confidence in the expansion of the CRT from 2002 to 2022. Of course, it must be noted that whether the residual trend may be part of a longer decadal cycle cannot be unambiguously determined from a 20-year time series.

Strengthening of trade winds and upwelling in the equatorial Pacific

Trade winds drive equatorial upwelling and the westward advection of nutrient-rich water from the eastern Pacific, leading to the formation of the CRT[27,35,36]. EMD analysis of the wind data shows that the easterly winds in the equatorial Pacific had strengthened from 2002 to 2022, which could lead to stronger westward currents and can partly explain the westward extension of the CRT (Fig. 5a). Indeed, EMD analysis of the SEC velocity time series reveals an increasing trend of SEC zonal velocity of ~0.14 m/s from 2002 to 2022 (Fig. 5b). Also, the intensified easterly winds observed here align well with the broader observation of a substantial strengthening of the equatorial easterly winds since the 1980s[18,20,37,38].

We further estimated the Ekman transport and divergence over the equatorial Pacific (see "Methods") and conducted an EMD analysis on the obtained time series. Within the range of 170° E–100° W, the total equatorial Ekman transport at 5° S increased, on average, by ~16.47 Sv from 2002 to 2022 (Fig. 6a), while a decrease of ~5.02 Sv for the total Ekman transport at 5° N in the same period is observed (Fig. 6b). The intensity of the equatorial upwelling, i.e., the total Ekman

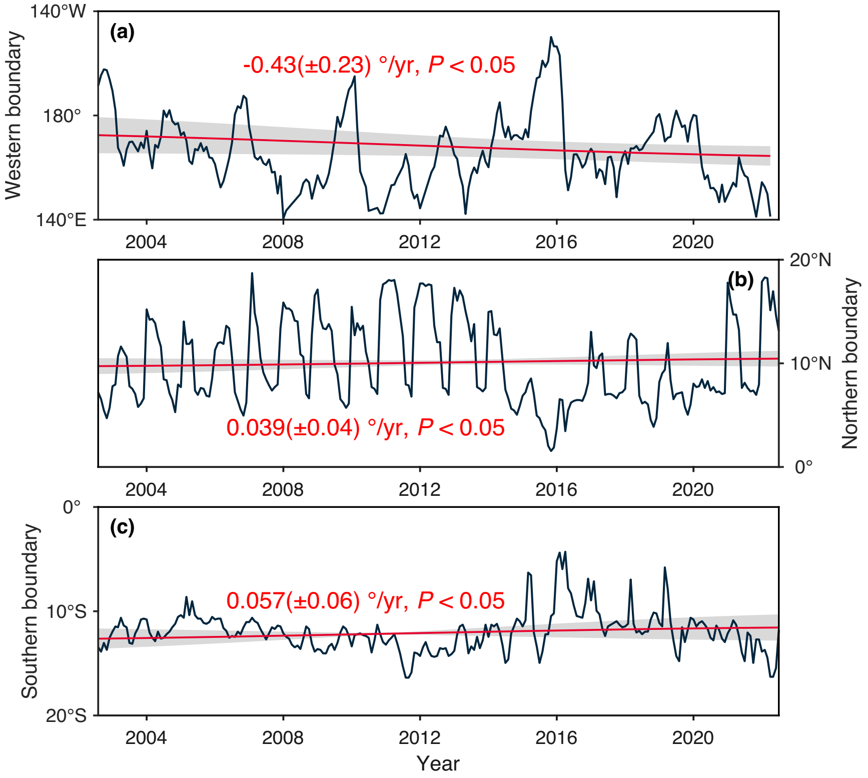

Fig. 3 | Long-term movement trends of the boundaries of the chlorophyll-rich tongue (CRT). Temporal variation of the (**a**) western, (**b**) northern, and (**c**) southern boundaries of the CRT from 2002 to 2022. Definitions of the boundaries are provided in “Methods”. The red line and gray shading represent the long-term trend and the 95% confidence limit via empirical mode decomposition analysis, as in Fig. 2d.

divergence, computed by summing up the southward and northward Ekman transport, exhibits an increasing trend of ~15.29 Sv over the investigated period (Fig. 6c). Note that this increasing number of the total Ekman divergence (~15.29 Sv) does not match the combination of those at the northern (~16.47 Sv) and the southern edges (~5.02 Sv), which is mainly due to the north-south asymmetry of surface equatorial current system[39,40] and neglect of the transport at the western edge[41]. In summary, the strengthened easterly winds resulted in intensified westward advection and upwelling in the equatorial Pacific from 2002 to 2022, providing a plausible explanation for the westward expansion of the CRT.

Discussion

The above analysis offers a compelling answer to the proposed question regarding the changes in the CRT in the equatorial Pacific, namely that the CRT did not shrink but expanded from 2002 to 2022. We found that, hidden beneath the most prominent high-frequency ENSO signal, there occurs a westward extending trend for the CRT in the equatorial Pacific Ocean. In the meantime, this finding suggests that the CRT and the two subtropical gyres to its south and north likely co-expanded over the past two decades. Such a simultaneous expansion, however, is not contradictory, as the North and South Pacific Subtropical Gyres expanded toward the northeast and southwest directions, respectively (Supplementary Fig. 4), while the CRT extended westward.

The expansion of the CRT implies a broader coverage of phytoplankton-rich water along the equator. As phytoplankton are a crucial part of ocean ecosystems, feeding zooplankton and thus living resources at higher trophic levels, the westward extending of the CRT possibly results in large-scale redistribution of certain species, influencing ecosystems and fisheries[9,42]. Also, as chlorophyll in phytoplankton absorbs solar light, a higher abundance of phytoplankton increases the absorption of solar radiation, leading to an enhanced heating rate at the ocean surface[43]. Therefore, changes in the spatial distribution of the CRT would lead to a redistribution of heat in the surface layer, influencing tropical climate, especially the amplitude and asymmetry of the ENSO[24,44]. Indeed, further quantification of these consequences of expanding CRT would require more dedicated efforts.

On the other hand, it is noticeable that our study period of 2002–2022 aligns with almost consecutive negative phases of the Pacific Decadal Oscillation (PDO)[45–47], suggesting that the detected expansion trend of the CRT may contain low-frequency variabilities. To explore potential links of the low-frequency variabilities of the CRT to the PDO, we adopted a mathematical approach of Stallone et al.[48] to symmetrically extrapolate the CRT area time series out of the boundaries, generating a new time series that is five times longer than the original one (see “Methods”). The decomposed decadal component of the CRT area after applying the EMD to this prolonged time series shows a significant negative correlation with the PDO in 2002–2022; meanwhile, there exists a weaker residual trend at a rate of 0.42 (±0.19) × 10^5 km^2/yr ($P < 0.05$) (Supplementary Fig. 5) compared to that calculated from the original time series (Fig. 2d). It suggests that the original 20-year CRT residual trend shown in Fig. 2d contains decadal signal to a large extent. Therefore, the observed westward expansion of the CRT from 2002 to 2022 seems mostly to result from naturally occurring internal variability related to the PDO. The weaker residual trend (0.42 × 10^5 km^2/yr), however, implies a potential linkage of the CRT expanding to climate change, particularly given that the CRT coincides with regions showing the highest signal-to-noise ratio when analyzing climate change-driven trends in ocean color[19]. Nevertheless, a truly decades-long CRT data record, rather than a mathematically prolonged time series, must be established to confidently attribute the expansion of the CRT extent to climate change.

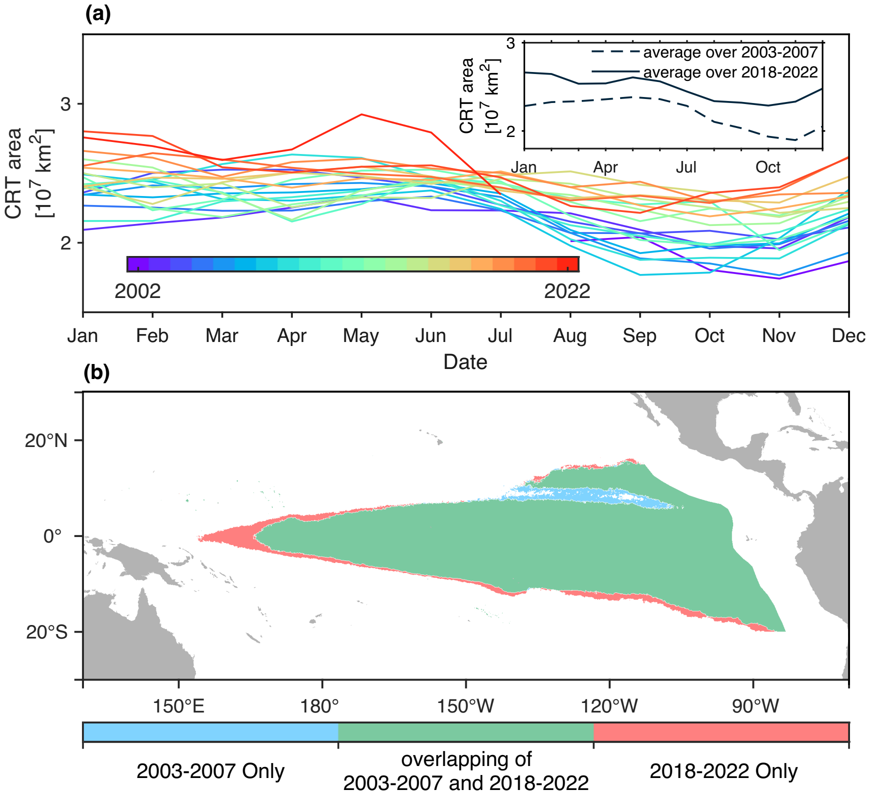

Fig. 4 | Illustration of the westward extension of the chlorophyll-rich tongue (CRT). a Evolution of the monthly CRT area from 2002 to 2022. The insert figure in (**a**) shows the comparison between the average annual cycle in 2003–2007 (the black dashed line) and that in 2018–2022 (the solid black line). **b** Comparison of the average CRT extent between the first (2003–2007, light blue patches) and the last five years (2018–2022, magenta patches) of the investigated period. Green areas represent the overlapped CRT extent in these two periods.

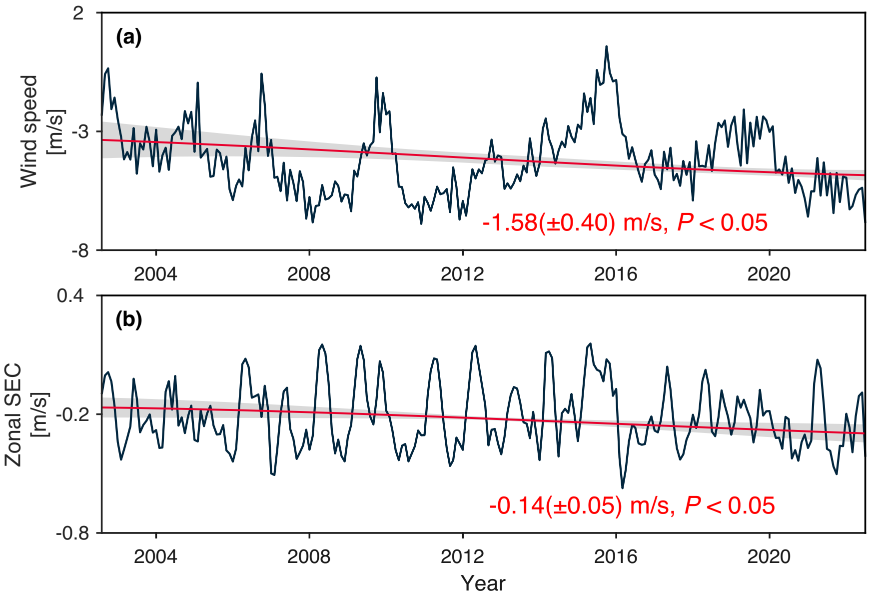

Fig. 5 | The easterly trade winds over the equatorial Pacific and the South Equatorial Current (SEC) strengthened from 2002 to 2022. Monthly variation of (**a**) the mean speed of the easterly trade winds and (**b**) the mean zonal velocity of SEC. Calculations of the mean speed and mean zonal velocity are described in "Methods". The red line and gray shading represent the long-term trend and the 95% confidence limit via empirical mode decomposition analysis, as in Fig. 2d. Negative trend values indicate strengthened easterly trades or westward SEC.

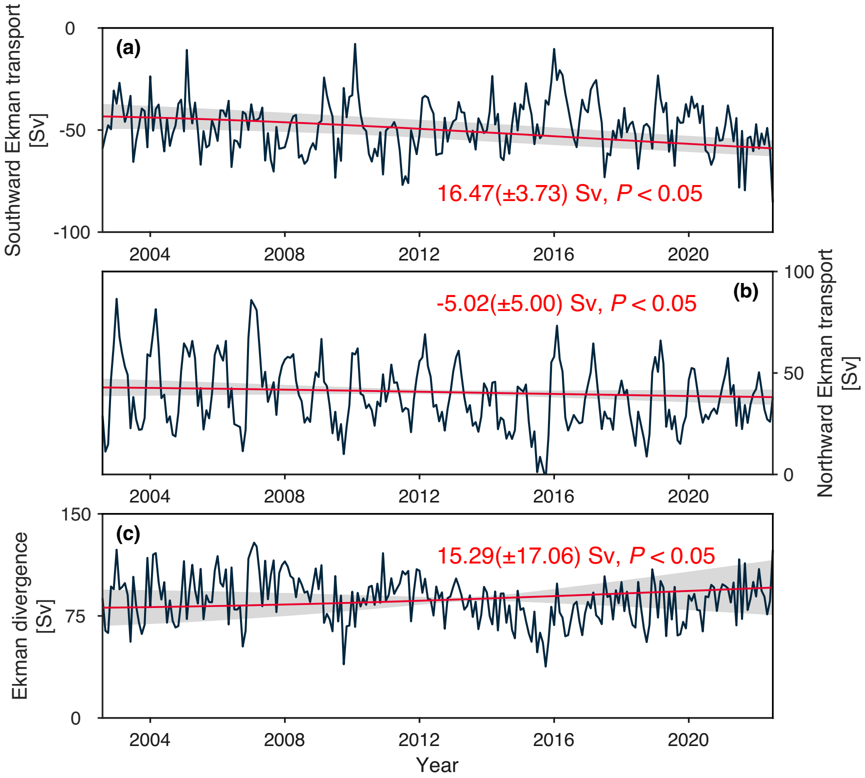

Fig. 6 | Intensified Ekman divergence in the equatorial Pacific from 2002 to 2022. Monthly variation of (**a**) the total southern Ekman transport calculated at 5° S, (**b**) the total northern Ekman transport calculated at 5° N, and (**c**) the Ekman divergence. The red line and gray shading represent the long-term trend and the 95% confidence limit via empirical mode decomposition analysis.

In addition, the ENSO-CRT area correlation observed in this effort and prior studies[2,24,29] suggests that if the occurrences of consecutive La Niña events increase under global warming as projected[14], the CRT will probably further extend to the west. Of course, the observed long-term trend of the CRT area highly depends on the data span used for trend analysis[25,49]. Thus, it is necessary to stress that the reported westward extending trend of the CRT is observed within a temporal period of 2002–2022. Nevertheless, our finding of the CRT westward expansion, never reported in previous observational and modeling efforts, highlights the importance of lower frequency variations hidden under major interannual variability of ENSO in the equatorial Pacific. Continued long-term observations spanning over 30 years or more would be essential for a more comprehensive and definitive understanding of the trend of CRT and its impacts[50,51].

Methods

Calculation of the area of the high chlorophyll tongue

The standard Level 3 monthly Chl products (version R2022.0), at a spatial resolution of 9 km, of Moderate Resolution Imaging Spectroradiometer (MODIS)-Aqua from August 2002 to July 2022 were acquired from NASA Ocean Color Web (https://oceancolor.gsfc.nasa.gov/l3/). The computation of the chlorophyll-rich tongue (CRT) area was confined to the open-ocean tropical Pacific region (20° N to 20° S). The eastern boundary was set ~1000 km from the shore, and a similar constraint was applied to the western boundary[7]. Pixels with Chl greater than 0.1 mg/m^3 within this region were identified as part of the CRT. The area of each pixel was computed based on its latitude, longitude, Earth radius, and the intervals of latitude and longitude between two adjacent pixels. Subsequently, the CRT area was determined by summing up the area of all pixels within the CRT.

An extended Chl monthly series from September 1997 to August 2023, distributed by the ESA Ocean Color project under the Climate Change Initiative (OC-CCI), was also acquired to supplement our analysis. The OC-CCI provides merged Chl products at 4 km spatial resolution from several ocean color missions, including MODIS-Aqua, the Sea-Viewing Wide Field-of-view Sensor, the Medium Resolution Imaging Spectrometer, and the Ocean and Land Color Instrument[52]. The OC-CCI monthly Chl products can be directly accessed via https://www.oceancolour.org/.

Definition of the boundaries of the CRT

The western boundary of the CRT for each month was identified as the longitude of the pixel where the meridional mean Chl between 1° N and 1° S from 150° W westward first declined to 0.1 mg/m^3. Note that the western boundary could be absent in some months when Chl in the entire Equatorial Pacific exceeds 0.1 mg/m^3, i.e., blank longitude values for these months. Most blank values were filled using cubic spline interpolation. However, those from May to September 2022, at the end of the time series, remain blank (see Fig. 3a) because it is unreasonable to do extrapolation. For the northern and southern boundaries of CRT in each month, we first computed the zonal mean Chl between 140° W and 150° W and established a latitudinal profile of mean Chl from 20° N to 20° S. We then screened the latitudinal profile and extracted the two latitudes with mean Chl of 0.1 mg/m^3 as the northern and southern boundaries.

Empirical mode decomposition for trend analysis

The Empirical Mode Decomposition (EMD) has demonstrated its efficacy in extracting intrinsic trends and natural variability from climate data in geophysical research[25,26,53,54]. Briefly, the original data is decomposed into a finite number of Intrinsic Mode Functions (IMFs), which correspond to the scale in the data ranging from the smallest to the largest, and the trend of the original data is defined as the average of the residual components from the decomposed IMFs. There is an upgraded version of the EMD called the Ensemble Empirical Mode Decomposition

(EEMD), aiming to solve potential drawbacks of the EMD by sifting an ensemble of white-noise added signal[34]. In this study, the EMD was attempted for all the time series involved in the CRT analysis. The EEMD was only carried out with the CRT area time series for comparison.

Here, in the sifting process of the EMD, the S stoppage was used as the stoppage criterion, producing five sets of IMFs with different S values ranging from 2 to 6 (Supplementary Fig. 1). The IMF1 and IMF2, with an average period < 2 years, were combined into the seasonal component of the CRT area; the IMF3 and IMF4, with an average period > 2 years, were combined into the interannual component; and the IMF5 and IMF6, with an average period > 8 years, emerging as the low-frequency signals, are most probably a result of over-sifting for such a time series of a limited span (20 years), and thus were combined with the IMF3 and IMF4 as the interannual component[26,28,55]. Finally, the residual components from these five sets of IMFs were averaged to derive the residual trend of the CRT area. A linear regression was then applied to this residual trend to obtain the changing rate of the CRT area in the given span of 2002–2022. In addition, the confidence limit serves as a standard measure for assessing the outcomes of EMD[56], which is defined as a range of standard deviations from the equally valid IMF sets. In this effort, the standard deviation was computed from five residual trend components, each generated with a different S stoppage criterion, with two standard deviations equivalent to a 95% confidence limit. In comparison, in the sifting process of the EEMD, the amplitude of added white noise was 1% of the standard deviation of the original data, and the ensemble number was 800.

In addition, to overcome the limitation of the short temporal span of the original CRT time series and to enable the decomposition of the decadal component of the CRT area, an anti-reflective extension algorithm[48] was used to generate a time series of the CRT area that is five times longer than the original one. The same EMD was then applied to this new time series, producing five sets of IMFs. The IMFs with an average period > 8 years contained physically meaningful signals for such a 120-year time series; they were no longer combined with the IMFs with an average period > 2 years (interannual component), but were extracted as decadal component (Supplementary Fig. 5).

Physical and chemical parameters in the tropical Pacific

Near-surface monthly mean currents (0.25° × 0.25° grid) were obtained from the Ocean Surface Current Analysis—Real time (OSCAR)[57]. The mean zonal velocity of the South Equatorial Current was then calculated for the tropical Pacific (5° S–5° N, 170° E–100° W) as done in a previous study[17].

The bi-monthly Multivariate ENSO Index v2 was from the National Oceanic and Atmospheric Administration (NOAA) Physical Sciences Laboratory (PSL)[58] (https://psl.noaa.gov/enso/mei/). The Pacific Decadal Oscillation (PDO) index was obtained from the National Centers for Environmental Information (NCEI)[46] (https://www.ncei.noaa.gov/access/monitoring/pdo/). We extracted the low-frequency (> 8 years) components of the PDO index by using an 8-year low-pass filter based on the fast Fourier transform filter.

The L3 gridded monthly mean sea surface wind speed and wind stress, at a spatial resolution of 0.25°, were retrieved from the Copernicus Marine Service (CMEMS), which is produced from the Near-Real-Time L2 Scatterometer product (https://marine.copernicus.eu/). The mean zonal wind was then calculated for the region of 5° S–5° N, 150° E - 150° W following Ma and Zhou[18].

Following Wyrtki[41], within the range of 170° E–100° W (covering a distance of ~10^4 km), the southward Ekman transport at 5° S (V^y) was estimated according to

$$V^y = \frac{\tau^x}{\rho f},$$

where τ^x is the zonal component of the wind stress, f represents the Coriolis parameter, and ρ is the density of seawater. The northward Ekman transport at 5° N was calculated following the same approach. The total Ekman divergence, i.e., the intensity of equatorial upwelling, was obtained by summing up the southward and northward Ekman transport.

Definition of the center of the Pacific Subtropical Gyre

The expansion or moving direction of the Pacific Subtropical Gyre (PSG) is characterized by the shift in its central position. Pixels featuring Chl values below 0.07 mg/m^3 were categorized into PSG[23]. The central position of PSG was calculated as[59]

$$\mathrm{X} = \frac{\sum_{i=1}^{n} X_i}{n}$$

$$\mathrm{Y} = \frac{\sum_{i=1}^{n} Y_i}{n}$$

where X_i and Y_i are the longitude and latitude of all pixels within PSG, respectively, while X and Y are the longitude and latitude representing the center of PSG.

Data availability

All the satellite measurements used in this effort can be directly accessed from the NASA Ocean Color Web (https://oceancolor.gsfc.nasa.gov/l3/) and the ESA OC-CCI Web (https://www.oceancolour.org/). The source data underlying results presented in Figures and Supplementary Figs. are provided in the spreadsheets in the Source Data file. Source data are provided with this paper.

Code availability

All codes are available at https://doi.org/10.5281/zenodo.14288695.

References

1. Chavez, F. P. & Barber, R. T. An estimate of new production in the equatorial Pacific. *Deep Sea Res. Part I Oceanogr. Res. Pap.* **34**, 1229–1243 (1987).
2. Chavez, F. P. et al. Biological and Chemical Response of the Equatorial Pacific Ocean to the 1997-98 El Niño. *Science* **286**, 2126–2131 (1999).
3. Chavez, F. P. & Toggweiler, J. R. Physical estimates of global new production: the upwelling contribution. In: Summerhayes, C. P., Emeis, K.-C., Angel, M. V., Smith, R. L., Zeitschel, B. (Eds.), *Upwelling in the Ocean: Modern Processes and Ancient Records*. Wiley, Chichester, pp. 313–320 (1995).
4. Koblentz-Mischke, O. I., Volkovinsky, V. V.& Kabanova, J. G. Plankton primary production of the world ocean. In: Wooster, W. S. (Ed.), *Scientific Exploration of the South Pacific*. National Academy of Sciences, DC, pp. 183-193 (1970).
5. Wyrtki, K. & Kilonsky, B. Mean water and current structure during the Hawaii-to-Tahiti shuttle experiment. *J. Phys. Oceanogr.* **14**, 242–254 (1984).
6. Nelson, D. M. & Landry, M. R. Regulation of phytoplankton production and upper-ocean biogeochemistry in the eastern equatorial Pacific: Introduction to results of the Equatorial Biocomplexity project. *Deep Sea Res. Part II Top. Stud. Oceanogr.* **58**, 277–283 (2011).
7. Pennington, J. T. et al. Primary production in the eastern tropical Pacific: A review. *Prog. Oceanogr.* **69**, 285–317 (2006).
8. Barber, R. T. & Chavez, F. P. Biological consequences of El Niño. *Science* **222**, 1203–1210 (1983).
9. Barber, R. T. & Chavez, F. P. Ocean variability in relation to living resources during the 1982–83 El Niño. *Nature* **319**, 279–285 (1986).

10. Blanchot, J., Borgne, R., Bouteiller, A. & Rodier, M. ENSO events and consequences on the nutrient planktonic biomass and production in the Western Pacific Tropical Ocean. In: *Proceedings of TOGA-COARE meeting*, 785–790 (1989).
11. Barber, R. T. & Kogelschatz, J. E. Nutrients and Productivity During the 1982/83 El Niño. *Elsevier Oceanogr. Ser.* **52**, 21–53 (1990).
12. Blanchot, J., Rodier, M. & Bouteiller, A. Effect of El Niño Southern Oscillation events on the distribution and abundance of phytoplankton in the Western Pacific Tropical Ocean along 165° E. *J. Plankton Res.* **14**, 137–156 (1992).
13. Geng, T. et al. Increased occurrences of consecutive La Niña events under global warming. *Nature* **619**, 774–781 (2023).
14. England, M. H. et al. Recent intensification of wind-driven circulation in the Pacific and the ongoing warming hiatus. *Nat. Clim. Chang.* **4**, 222–227 (2014).
15. Wang, M., Xie, S.-P., Sasaki, H., Nonaka, M. & Du, Y. Intensification of Pacific tropical instability waves over the recent three decades. *Nat. Clim. Chang.* **14**, 163–170 (2024).
16. Cai, W. et al. Increased variability of eastern Pacific El Niño under greenhouse warming. *Nature* **564**, 201–206 (2018).
17. Hsin, Y.-C. Trends of the pathways and intensities of surface equatorial current system in the North Pacific Ocean. *J. Clim.* **29**, 6693–6710 (2016).
18. Ma, S. & Zhou, T. Robust Strengthening and Westward Shift of the Tropical Pacific Walker Circulation during 1979–2012: A Comparison of 7 Sets of Reanalysis Data and 26 CMIP5 Models. *J. Clim.* **29**, 3097–3118 (2016).
19. Cael, B. B. et al. Global climate-change trends detected in indicators of ocean ecology. *Nature* **619**, 511–554 (2023).
20. McClain, C. R., Signorini, S. R. & Christian, J. R. Subtropical gyre variability observed by ocean-color satellites. *Deep Sea Res. Part II Top. Stud. Oceanogr.* **51**, 281–301 (2004).
21. Signorini, S. R., Franz, B. A. & McClain, C. R. Chlorophyll variability in the oligotrophic gyres: mechanisms, seasonality and trends. *Front. Mar. Sci.* **2**, 1 (2015).
22. Dai, M. et al. Upper Ocean Biogeochemistry of the Oligotrophic North Pacific Subtropical Gyre: From Nutrient Sources to Carbon Export. *Rev. Geophys.* **61**, e2022RG000800 (2023).
23. Polovina, J. J., Howell, E. A. & Abecassis, M. Ocean's least productive waters are expanding. *Geophys. Res. Lett.* **35**, L03618 (2008).
24. Timmermann, A. & Jin, F. F. Phytoplankton influences on tropical climate. *Geophys. Res. Lett.* **29**, 1–4 (2002).
25. Wu, Z., Huang, N. E., Long, S. R. & Peng, C.-K. On the trend, detrending, and variability of nonlinear and nonstationary time series. *Proc. Natl Acad. Sci. USA.* **104**, 14889–14894 (2007).
26. Serio, C., Montzka, S. A., Masiello, G. & Carbone, V. Trend and multi-frequency analysis through empirical mode decomposition: An application to a 20-year record of atmospheric carbonyl sulfide measurements. *J. Geophys. Re. Atmo.* **128**, e2022JD038207 (2023).
27. Radenac, M.-H., Messié, M., Léger, F. & Bosc, C. A very oligotrophic zone observed from space in the equatorial Pacific warm pool. *Remote Sens. Environ.* **134**, 224–233 (2013).
28. Keerthi, M. G., Prend, C. J., Aumont, O. & Lévy, M. Annual variations in phytoplankton biomass driven by small-scale physical processes. *Nat. Geosci.* **15**, 1027–1033 (2022).
29. Browning, T. J. et al. Persistent equatorial Pacific iron limitation under ENSO forcing. *Nature* **621**, 330–335 (2023).
30. Drenkard, E. J. & Karnauskas, K. B. Strengthening of the Pacific Equatorial Undercurrent in the SODA Reanalysis: Mechanisms, Ocean Dynamics, and Implications. *J. Clim.* **27**, 2405–2416 (2014).
31. Messié, M. & Chavez, F. P. A global analysis of ENSO synchrony: The oceans' biological response to physical forcing. *J. Geophys. Res. Ocean.* **117**, C09001 (2012).
32. Turk, D., McPhaden, M. J., Busalacchi, A. J. & Lewis, M. R. Remotely sensed biological production in the equatorial pacific. *Science* **293**, 471–474 (2001).
33. Radenac, M. H. et al. Modeled and observed impacts of the 1997–1998 El Niño on nitrate and new production in the equatorial Pacific. *J. Geophys. Res. Ocean.* **106**, 26879–26898 (2001).
34. Wu, Z. & Huang, N. E. Ensemble empirical mode decomposition: A noise-assisted data analysis method. *Adv. Adapt. Data Anal.* **1**, 1–41 (2009).
35. Messié, M. & Radenac, M.-H. Seasonal variability of the surface chlorophyll in the western tropical Pacific from SeaWiFS data. *Deep Sea Res. Part I Oceanogr. Res. Pap.* **53**, 1581–1600 (2006).
36. Chai, F., Lindley, S. T. & Barber, R. T. Origin and maintenance of a high nitrate condition in the equatorial Pacific. *Deep Sea Res. Part II Top. Stud. Oceanogr.* **43**, 1031–1064 (1996).
37. Dong, B. & Lu, R. Interdecadal enhancement of the walker circulation over the Tropical Pacific in the late 1990s. *Adv. Atmos. Sci.* **30**, 247–262 (2013).
38. McGregor, S. et al. Recent Walker circulation strengthening and Pacific cooling amplified by Atlantic warming. *Nat. Clim. Chang.* **4**, 888–892 (2014).
39. Reverdin, G., Frankignoul, C., Kestenare, E. & McPhaden, M. J. Seasonal variability in the surface currents of the equatorial Pacific. *J. Geophys. Res. Ocean.* **99**, 20323–20344 (1994).
40. Hsin, Y. C. & Qiu, B. Seasonal fluctuations of the surface North Equatorial Countercurrent (NECC) across the Pacific basin. *J. Geophys. Res. Ocean.* **117**, C06001 (2012).
41. Wyrtki, K. An estimate of equatorial upwelling in the pacific. *J. Phys. Oceanogr.* **11**, 1205–1214 (1981).
42. Domokos, R. Influence of El Niño-Southern Oscillation on bigeye and yellowfin tuna longline catch per unit effort in the equatorial Pacific. *Fish. Oceanogr.* **32**, 527–540 (2023).
43. Sathyendranath, S. et al. Biological control of surface temperature in the Arabian Sea. *Nature* **349**, 54–56 (1991).
44. Lewis, M. R., Carr, M.-E., Feldman, G. C., Esaias, W. & McClain, C. Influence of penetrating solar radiation on the heat budget of the equatorial Pacific Ocean. *Nature* **347**, 543–545 (1990).
45. Gu, D. & Philander, S. G. H. Interdecadal climate fluctuations that depend on exchanges between the tropics and extratropics. *Science* **275**, 805–807 (1997).
46. Zhang, Y., Wallace, J. M. & Battisti, D. S. ENSO-like interdecadal variability: 1900–93. *J. Clim.* **10**, 1004–1020 (1997).
47. Staten, P. W. et al. Recent tropical expansion: Natural variability or forced response? *J. Clim.* **32**, 1551–1571 (2019).
48. Stallone, A., Cicone, A. & Materassi, M. New insights and best practices for the successful use of Empirical Mode Decomposition, Iterative Filtering and derived algorithms. *Sci. Rep.* **10**, 15161 (2020).
49. Eriksen, T. & Rehman, N.u. Data-driven nonstationary signal decomposition approaches: A comparative analysis. *Sci. Rep.* **13**, 1798 (2023).
50. Henson, S. A. et al. Detection of anthropogenic climate change in satellite records of ocean chlorophyll and productivity. *Biogeosciences* **7**, 621–640 (2010).
51. Gregg, W. W. & Rousseaux, C. S. Decadal trends in global pelagic ocean chlorophyll: A new assessment integrating multiple satellites, in situ data, and models. *J. Geophys. Res. Oceans* **119**, 5921–5933 (2014).
52. Sathyendranath, S. et al. An ocean-colour time series for use in climate studies: The experience of the ocean-colour climate change initiative (OC-CCI). *Sensors* **19**, 4285 (2019).
53. Huang, N. E., Shen, Z. & Long, S. R. A new view of nonlinear water waves: The Hilbert spectrum. *Annu. Rev. Fluid Mech.* **31**, 417–457 (1999).
54. Huang, N. E. et al. The empirical mode decomposition and the Hilbert spectrum for nonlinear and non-stationary time series

analysis. *Proc. R. Soc. Lond. Ser. A Math. Phys. Eng. Sci.* **454**, 903–995 (1998).

55. Ji, K. et al. Enhanced North Pacific Victoria mode in a warming climate. *npj Clim. Atmos. Sci.* **7**, 49 (2024).
56. Huang, N. E. et al. A confidence limit for the empirical mode decomposition and Hilbert spectral analysis. *Proc. R. Soc. Lond. Ser. A Math. Phys. Eng. Sci.* **459**, 2317–2345 (2003).
57. Bonjean, F. & Lagerloef, G. S. E. Diagnostic model and analysis of the surface currents in the tropical pacific ocean. *J. Phys. Oceanogr.* **32**, 2938–2954 (2002).
58. Wolter, K. & Timlin, M. S. El Niño/Southern Oscillation behaviour since 1871 as diagnosed in an extended multivariate ENSO index (MEI.ext). *Int. J. Climatol.* **31**, 1074–1087 (2011).
59. Chen, X., Cao, J., Chen, Y., Liu, B. & Tian, S. Effect of the Kuroshio on the Spatial Distribution of the Red Flying Squid Ommastrephes Bartramii in the Northwest Pacific Ocean. *Bull. Mar. Sci.* **88**, 63–71 (2012).

Acknowledgements

We sincerely appreciate the constructive comments and suggestions provided by four anonymous reviewers, which significantly improved this manuscript. Z. L. and X.Y. acknowledge funding from the National Key Research and Development Program of China (2022YFB3901703, 2022YFC3104903). S. S. and Z. L. acknowledge support from the National Natural Science Foundation of China (42430107, 41890803, and 42250710150). The authors thank the Ocean Biology Processing Group of NASA for processing and distributing the ocean color products of MODIS-Aqua.

Author contributions

S. P. and X. Y. performed the data analysis and wrote the original draft; S. S. conceived the study (conceptualization and methodology); X. Y., S. S., and Z. L. led the revisions of the manuscript. H. L., X. L., and M. D. contributed to the manuscript review and editing. All authors participated in interpreting the results and refinement of the paper.

Competing interests

The authors declare no competing interests.

Additional information

Supplementary information The online version contains supplementary material available at https://doi.org/10.1038/s41467-024-55650-8.

Correspondence and requests for materials should be addressed to Shaoling Shang.

Peer review information *Nature Communications* thanks Aleksandra Cherkasheva who co-reviewed with Artur PalaczHervé Demarcq and the other, anonymous, reviewer for their contribution to the peer review of this work. A peer review file is available.

Reprints and permissions information is available at http://www.nature.com/reprints